Supplementary Material

3D Printed Hydrogel Scaffolds for Meniscal Implant Application: Photo-crosslinkable Urethane-Based Poly(Ethylene Glycol) as a case study.

Ozge Begum Akalin[a] , Andrada Serafim[b], Izabela-Cristina Stancu[b], Catherine Van Der Straeten[c,d] , Peter Dubruel[a,*]

[a] Polymer Chemistry & Biomaterials Research Group, Center of Macromolecular Chemistry (CMAC), Ghent University, Krijgslaan 281, Building S4-bis, B-9000 Ghent, Belgium
[b] Advanced Polymer Materials Group, University Politehnica of Bucharest, Bucharest, Romania
[c] International Society of Technology in Arthroplasty, 1246 P Street, Sacramento, CA 95814, USA.
[d] HIRUZ - University Hospital Ghent, C. Heymanslaan 10, 9000 Gent, Belgium

* Corresponding author: Peter.Dubruel@ugent.be

1. Synthesis of the AUP hydrogel precursors

AUPs with five different molar masses were synthesized by a two-step modification of PEG (1000, 2000, 4000, 6000, 8000 g/mol). In the first reaction step, PEG was reacted with two equivalents of IPDI resulting in the formation of a PEG-IPDI intermediate product. In the second reaction step, the PEG-IPDI intermediate product was reacted with two equivalents of an oligoethylene oxide monoacrylate (OEOacr) end-capping agent. The chemical structure of the obtained products (AUPPEG1K, AUPPEG2K, AUPPEG4K, AUPPEG6K, and AUPPEG8K) and the backbone molar masses are presented in Figure S1.

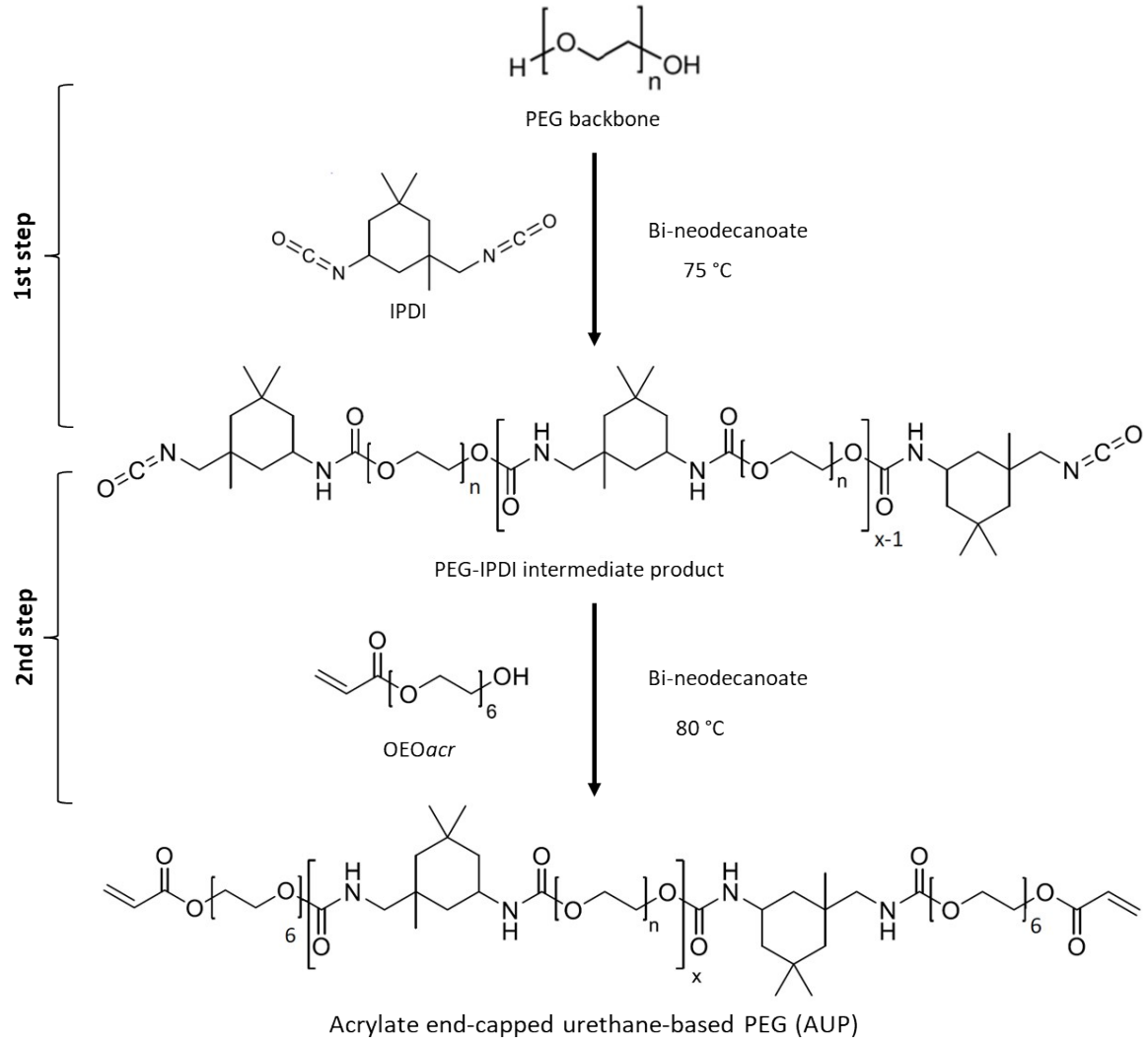

Where n ≈ 23 for AUPPEG1K and x ≈ 3
45 for AUPPEG2K
91 for AUPPEG4K
136 for AUPPEG6K
182 for AUPPEG8K

Figure S1. Reaction scheme of AUP synthesis.

2. Fourier Transform Infrared (FTIR) spectroscopy

Figure S2 shows the FTIR spectra of the five AUP products obtained. First, the characteristic bands for the urethane groups were observed in the spectra, including the N-H stretching (V_{N-H} at 3330 cm^{-1}), the carbonyl stretching ($V_{C=O}$ at 1710 cm^{-1}), the amide II (N-H bending vibration at 1540 cm^{-1}), and the amide III (C-N stretching 1300 cm^{-1}), which confirms the urethanization of PEG [1]. In addition, the absorption bands at 1635 cm^{-1} and 1200 cm^{-1} corresponding, respectively, to the C=C stretching of the acrylate groups and the C-O stretching of the acrylate esters can also be observed. From the highlighted area of the spectra (Figure S2B), it is obvious that the intensity of the bands decreased with an increasing molar mass due to a decrease in the concentration of the corresponding functionalities.

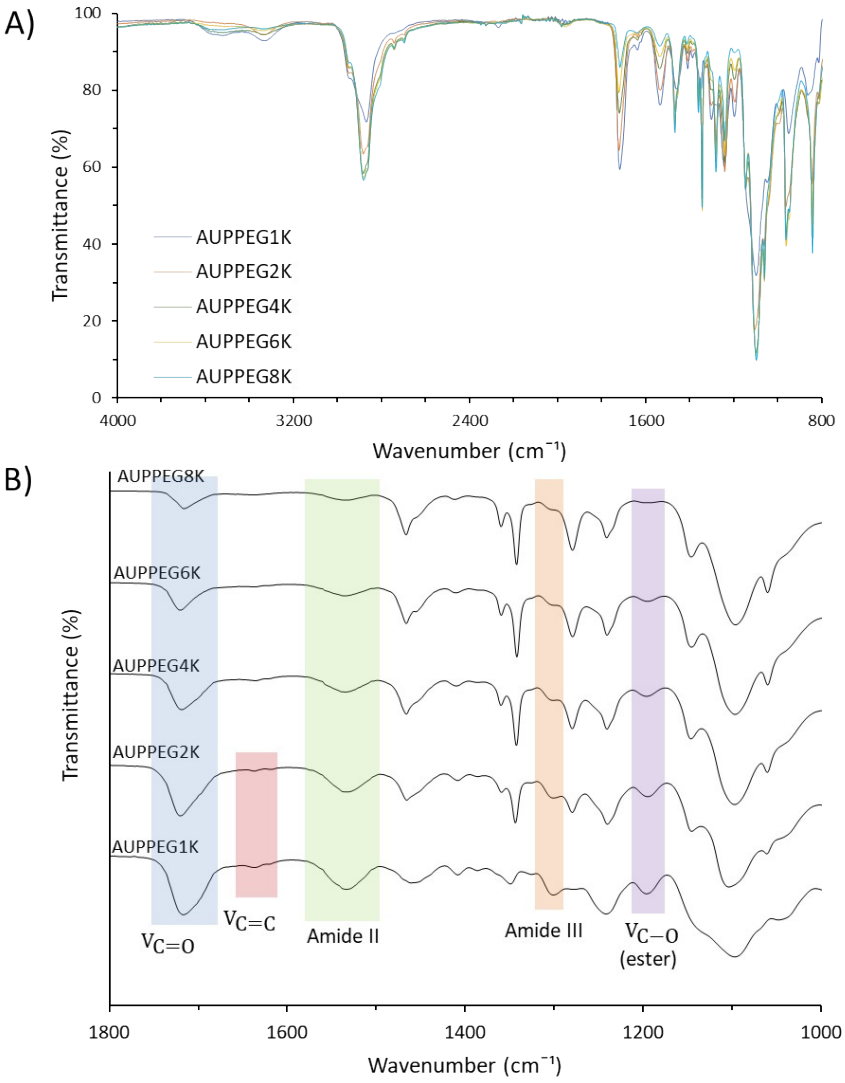

Figure S2. FTIR spectra of the different AUPs. A) stacked FTIR spectra in the range of 4000-800 cm^{-1} and B) in the range of 1800-1000 cm^{-1}.

3. Nuclear magnetic resonance (^{1}H-NMR) spectroscopy

All AUPs were analyzed via ^{1}H-NMR spectroscopy (Bruker Avance 400 MHz Spectrometer). They were dissolved in deuterated chloroform ($CDCl_3$, Euriso-Top) prior to analysis. The spectra were analyzed using the MestReNova software (version 6.0.2). The ^{1}H-NMR spectra of the final AUP products, shown in Figure S3A, were consistent with each other. Additionally, a reduction in the signal intensities of the acrylate AUP protons was observed with an increase in the AUP molar mass. This can be explained by the decrease in the concentration of the corresponding protons with an increasing AUP molar mass.

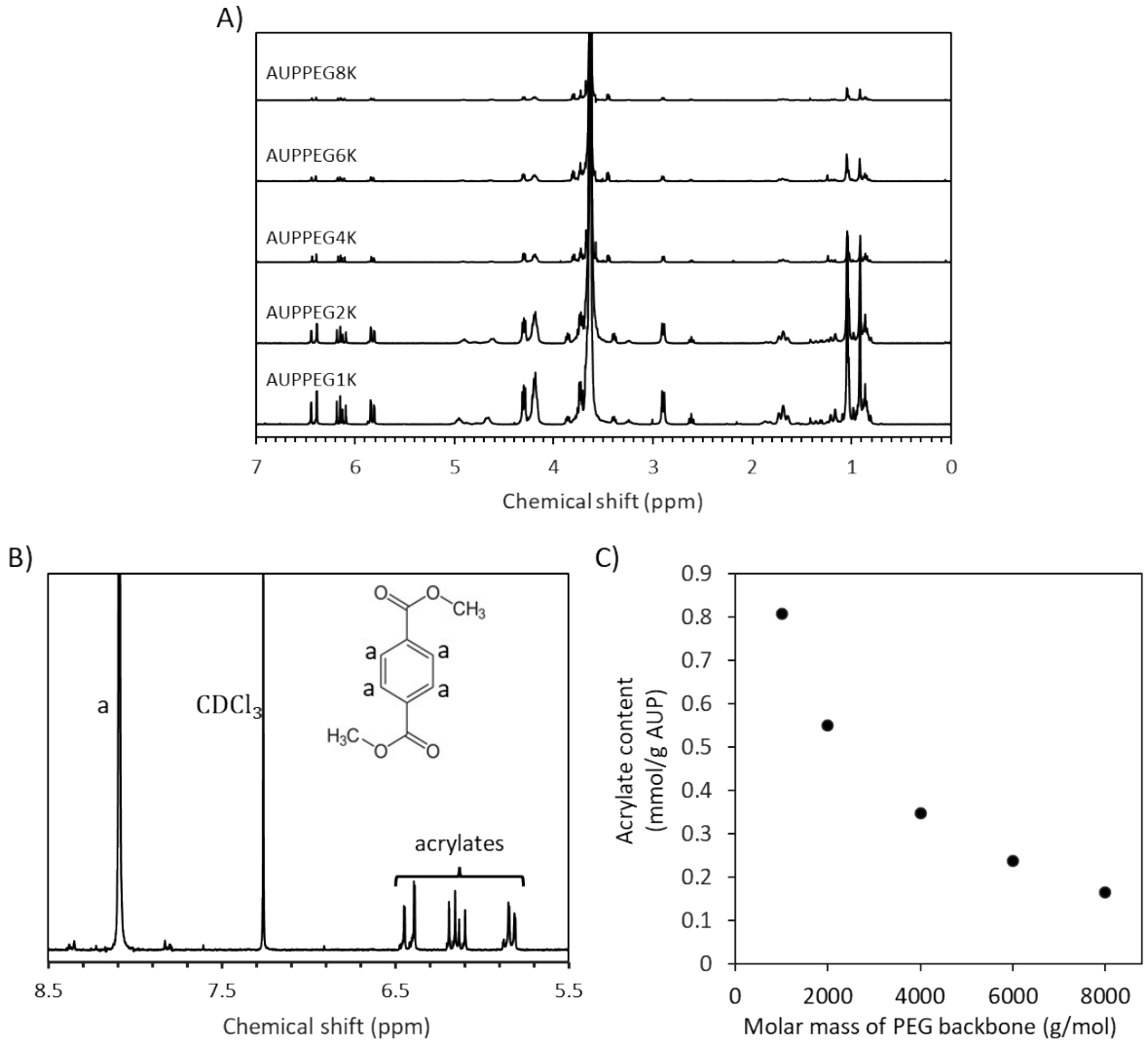

Figure S3. A) ^{1}H-NMR spectra of all AUPs. B) ^{1}H-NMR spectrum of AUPPEG4K in the presence of the DMT standard. C) Calculated acrylate contents of the different AUPs as a function of the PEG backbone molar mass.

The exact acrylate content of the AUPs was calculated by adding a specific amount of an appropriate standard to the solutions of the AUPs before the ^{1}H-NMR analysis. As a standard compound, dimethyl

terephthalate (DMT) was used to calculate the acrylate content of the AUPs. Particularly, the signal of the benzene protons from this compound was used for the acrylate content calculation since this signal did not interfere with the spectra of the AUPs. The acrylate content was calculated using Equation S1 and the ^{1}H-NMR spectrum of the AUPs containing DMT (Figure S3B).

$$M_{acr} = \frac{I_{\delta = 5.8ppm} + I_{\delta = 6.1ppm} + I_{\delta = 6.4ppm}}{I_{\delta = 8ppm}} x \frac{N_{H,\,\delta = 8ppm}}{N_{\delta = 5.8ppm} + N_{\delta = 6.1ppm} + N_{\delta = 6.4ppm}} x \frac{W_{DMT}}{MW_{DMT}} x \frac{1000}{W_{AUP}}$$

(Equation S1)

Where, M_{acr} is the content of acrylates in the polymers (mmol acrylate/g AUP), $(I_{\delta = 5.8ppm} + I_{\delta = 6.1ppm} + I_{\delta = 6.4ppm})$ is the sum of the integrals of the signals corresponding to the acrylate protons, $I_{\delta = 8ppm}$ is the integral of the signal attributed to the benzene protons in DMT, $(N_{\delta = 5.8ppm} + N_{\delta = 6.1ppm} + N_{\delta = 6.4ppm})$ is the number of protons in acrylate end group, $N_{H,\,\delta = 8ppm}$ is the number of protons in the benzene ring of DMT, MW_{DMT} is the molar mass of DMT (g/mol), W_{DMT} and W_{AUP} are the weights of DMT (g) and AUP (g) added in the NMR solutions, respectively.

4. Determination of the degree of substitution (DS)

The DS of AUPs is the percentual amount of hydroxyl groups in PEG (the AUP backbone) that are converted into acrylate groups during the AUP synthesis. To obtain the DS of AUPs, the hydroxyl content of PEG first needed to be quantified. For this purpose, trichloroacetyl isocyanate (TAIC) was used as an in situ derivatization reagent, as previously explained [2]. TAIC-derivatized PEG was quantified by the additional signal ($\delta = 8.6\ ppm$) corresponding to the imide protons in Figure S4. As expected, a reduction in the signal intensities was observed with the PEG molar mass increase, which could be attributed to the decrease in the concentration of the corresponding protons.

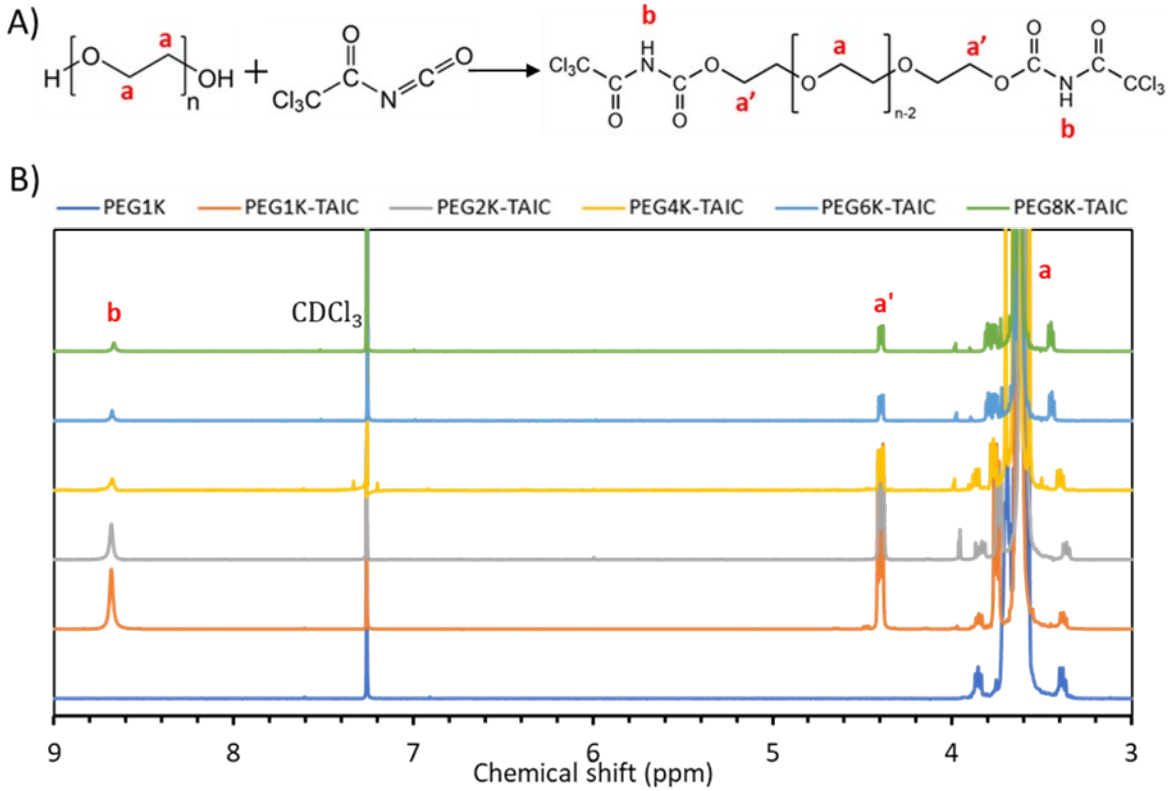

Figure S4. Quantification of the hydroxyl content of the backbone (PEG). A) The reaction of TAIC-derivatization of PEG. B)^{1}H-NMR spectra of TAIC-derivatized PEGs.

After quantifying the hydroxyl functionality of the applied PEGs (the AUP backbone) with different molar masses via ^{1}H-NMR using TAIC, the consumed hydroxyl content of PEGs during AUP synthesis was determined. This value is obtained by multiplying the PEG hydroxyl functionality and the initial hydroxyl content in AUP synthesis (In Table S1, the value of the first column times the value of the second column gives the value of the third column). The latter was defined as the mol of -OH consumed with respect to the initial PEG amount during the AUP synthesis, divided by the amount of AUP (g) obtained at the end. After finding the consumed -OH content during AUP synthesis, the amount of acrylation obtained via ^{1}H-NMR using the standard DMT, was recorded to find the so-called degree of substitution (DS) values of

AUPs. This value was specified as the amount (expressed in %) of hydroxyl groups in PEG that were replaced by the acrylate groups at the end of AUP synthesis. DS values of AUPs were calculated by dividing the acrylate content of AUPs by the consumed hydroxyl content. These values are shown in Table S1.

Table S1. Degree of Substitution of AUPs for different backbone molar masses as obtained via ^{1}H-NMR

Polymer	PEG Hydroxyl Functionality via TAIC-NMR (%)	Initial Hydroxyl Content ($\frac{mmol\ OH}{g\ AUP}$)	Consumed Hydroxyl Content ($\frac{mmol\ OH}{g\ AUP}$)	AUP Acrylate Content via DMT-NMR ($\frac{mmol\ acrylate}{g\ AUP}$)	Degree of Substitution (DS (%))
AUPPEG1K	93	0.94	0.87	0.81	93
AUPPEG2K	94	0.64	0.6	0.55	92
AUPPEG4K	90	0.39	0.35	0.34	97
AUPPEG6K	87	0.29	0.25	0.24	96
AUPPEG8K	83	0.22	0.18	0.17	94

For all developed AUPs, DS values between 92-97% are obtained. This indicates a successful reaction, irrespective of the molar mass of the PEG applied. Therefore, no further attempts were pursued to increase the obtained DS values.

5. Gel permeation chromatography

All peaks could be assigned by comparing the chromatograms of the final products to the reagents (dashed lines) in Figure S5. The numbers (2 to 4) indicate the different fractions observed in the chromatogram of the final AUPs. The fragments 2, 3 and 4 are attributed to the AUP molecules containing 1, 2 and 3 PEG macrodiols, respectively. The repeating units (indicated with "x" in Figure S1) equal approximately 3 for all AUPs. On the other hand, fragment 1 in the GPC chromatogram of AUPPEG2K probably corresponds to the adduct presence in AUPs, in which the unreacted diisocyanates after the first reaction step resulted in the formation of by-adducts by reacting with the end-capping agent OEO_{acr} in a 1:2 stoichiometric ratio in the second step of the reaction [3], such as OEO_{acr}-IPDI-OEO_{acr}. This broad peak of the adduct (indicated as 1) can be explained by the relatively high dispersity of OEO_{acr}, as shown in the light grey dashed line.

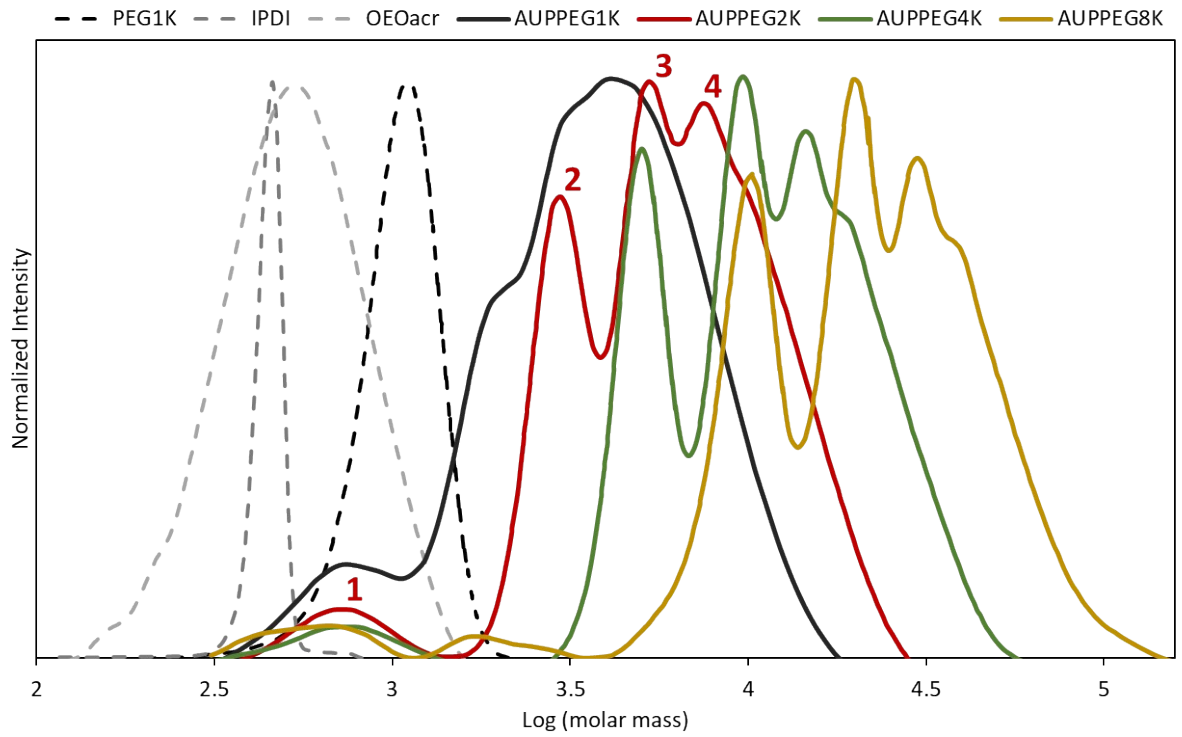

Figure S5. GPC chromatogram of reagents (PEG 1000 g/mol, IPDI and end-capping agent OEOacr) and the final products AUPPEG1K, AUPPEG2K, AUPPEG4K and AUPPEG8K. The numbered fragments (2-4) of AUPPEG2K correspond to the different "PEG-IPDI" repeating units, and fragment 1 corresponds to the by-adduct, OEO_{acr}-IPDI-OEO_{acr}. PEG (1000 g/mol) is added as a reference to guide the eye of the viewer.

The final molar mass of AUPs was more than twice that of PEG backbone molar mass. This can be explained by the repetition of "PEG-IPDI" units due to using a bismuth-based catalyst during the

synthesis of AUP hydrogel precursors. Although a bismuth-based catalyst was selected due to its low toxicity [4], its low selectivity can cause the repetition of the “PEG-IPDI” units, where IPDI is a non-symmetrical diisocyanate consisting of a primary and secondary isocyanate group. During the urethanization reaction, the isocyanate group of IPDI that is reacted depends on the catalyst type, the temperature, and the orientation of the substituents on the IPDI cyclohexane ring [5]. Particularly, the selectivity of Bi-based catalysts is low compared to their alternatives, such as Zn [5]. A lower selectivity of the catalyst causes the reaction of a certain amount of both the primary and the secondary isocyanate groups of IPDI in the first reaction step, leading to the repetition of the “PEG-IPDI” units. Thus, an increase in the molar mass and molar mass distribution is observed.

6. Characterization of the AUP thermal properties

6.1 Thermogravimetric analysis (TGA)

TGA was utilized to monitor the thermal degradation process by measuring the mass loss of the material as a function of an increasing temperature. This allowed a determination of the material's thermal stability and degradation temperature (T_d). For this purpose, AUPs were heated from 35 °C to 700 °C with a ramp of 10 °C/min under a flow of nitrogen gas. The TGA curves of the AUPs are presented in Figure S6.

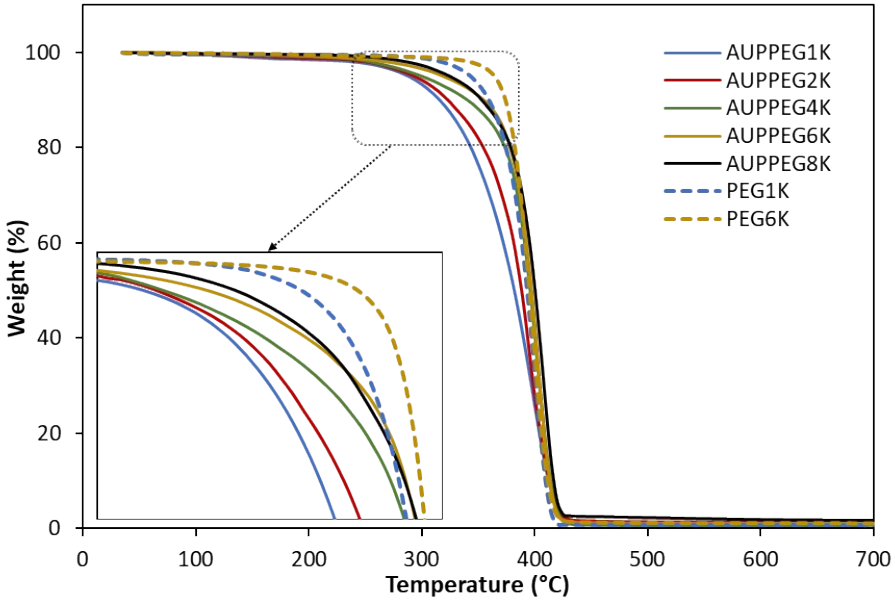

Figure S6. TGA curves of developed AUPs.

The TGA analyses confirmed that the AUPs were stable with a negligible mass loss (1%) until 210 °C. In addition, all AUPs undergo a single step degradation, a rapid mass loss due to thermal degradation at temperatures higher than 300 °C. When the temperature is increased beyond 300 °C, the onset of decomposition is observed mainly due to the decomposition of the PEG segments, which is consistent with previous studies on PEG-based polyurethanes [6]. The high thermal stability of AUPs can be explained by the formation of hydrogen bonding involving urethane and ester linkages. In addition, this high thermal stability allows the AUPs to be used as a starting material for the 3D printing process in the printing temperature range of 55 – 80 °C without any risk for thermal degradation. According to the obtained TGA curves shown in Figure S6, the positive influence of an increase in PEG backbone length on thermal stability is clear. This stability of the herein developed urethane-containing hydrogel precursors depends on an increase in chain entanglements.

6.2 Differential scanning Calorimetry (DSC)

Since AUPs are semi-crystalline polymers, a conventional DSC analysis was conducted to acquire the peak melting and crystallization temperatures (T_m and T_c, respectively) of the AUPs. For the DSC analysis, the AUPs were first heated to 80 °C to erase their thermal history, then cooled to 10 °C with a controlled cooling rate of 10 °C/min. Subsequently, a heating cycle was applied to the polymers, where they were heated from 10 °C up to 80 °C with a controlled heating rate of 10 °C/min. The thermograms of all AUPs with the cooling and heating cycles are shown in Figure S7.

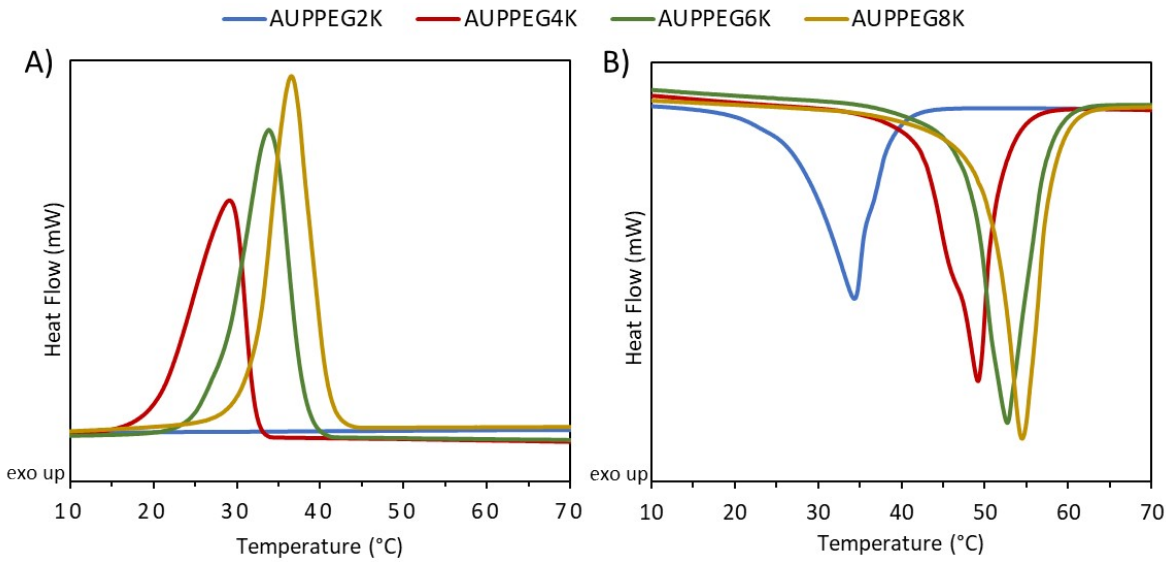

Figure S7. DSC thermograms of different AUPs. A) crystallization exotherms in the cooling cycle. B) melting endotherms in the heating cycle.

In this study, AUPPEG1K was excluded from the thermograms since exothermic and endothermic peaks were not observed in the applied temperature range. This can be explained by the liquid state of this polymer at room temperature, where the glass transition temperature of AUPPEG1K was below 0 °C and obtained by the mid-point of the step change of heat capacity while the polymer was heated (-47.2 °C). The focus of our research continued on the remaining AUPs except AUPPEG1K due to the application purposes.

All AUPs except AUPPEG2K indicated a single exothermic peak between 20 and 50 °C due to the crystallization of PEG segments during cooling [7]. Although no crystallization exotherm was observed for the AUPPEG2K in the cooling cycle, the presence of the melting endotherm in the subsequent heating cycle (Figure S7B) indicates that it underwent isothermal crystallization at 10 °C. Furthermore, a melting endotherm below 70 °C in the heating cycle was observed for all AUPs. The maximum of these exothermic and endothermic peaks was exhibited as the crystallization and the melting temperature (T_c and T_m), respectively.

7. Evaluation of AUP polymer melts viscosity via rheology

AUPs with a PEG backbone molar mass of 2000, 4000 and 8000 g/mol were evaluated for their melt viscosities. The measurements were performed at a strain of 0.1 % and a frequency of 1 Hz, as these values were within the linear viscoelastic range of the polymers.

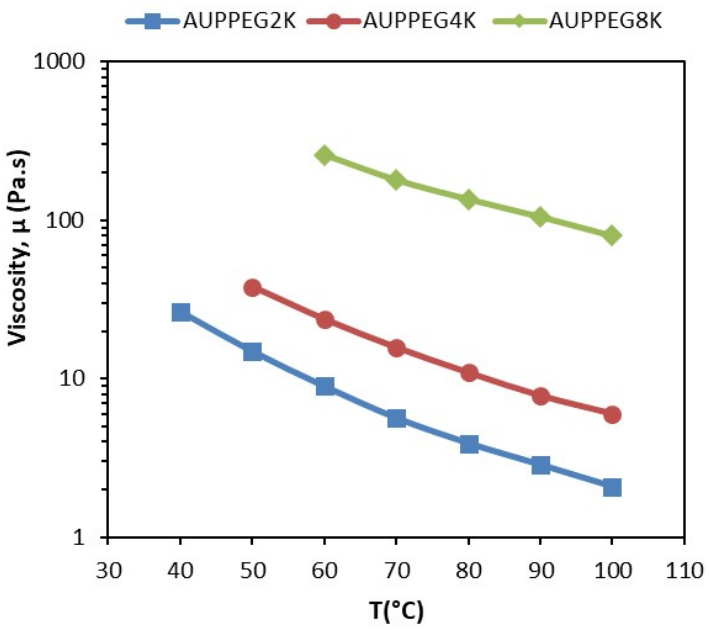

Figure S8. Complex viscosities of different AUPs as a function of temperature.

Figure S8 represents the effect of temperature on the viscosities of the AUP melts. In the analyzed temperature range, the viscosity of the AUP polymer melts ranged from 2 to 260 Pa s. The viscosity range of AUP polymer melts was in agreement with Guo et al., where the molar mass of 10-40 kg/mol PLGA was properly printed using the 3D-Bioplotter in a viscosity range of 1-100 Pa s [8]. Additionally, as anticipated, the temperature increase resulted in a decrease in the viscosities of the AUP melts. This decreasing viscosity trend of the AUP melts upon increasing temperature is in agreement with previous findings in the literature [9,10]. This finding can be explained by the higher mobility of the molecules upon temperature increase, resulting in a reduced viscosity. Lastly, an increase in molar mass, going from AUPPEG2K to AUPPEG8K, increased the viscosity of the AUP melts, as expected. This result is due to the fact that polymers with higher molar mass have more chain entanglements, leading to a stronger flow resistance, reflected by an increased viscosity.

8. The effect of the printing speed, printing pressure and photo-initiator addition on the properties of AUP scaffolds

8.1 Effect of printing speed and printing pressure

For the scaffolds based on AUPPEG8K, neither the printing speed nor the pressure had a significant effect (both $p > 0.05$) on the strut diameters (Figure S9). A printing pressure of 3 or 5 bar combined with printing speeds of 250 or 500 mm/min both give an almost perfect match with the applied needle diameter (250 µm).

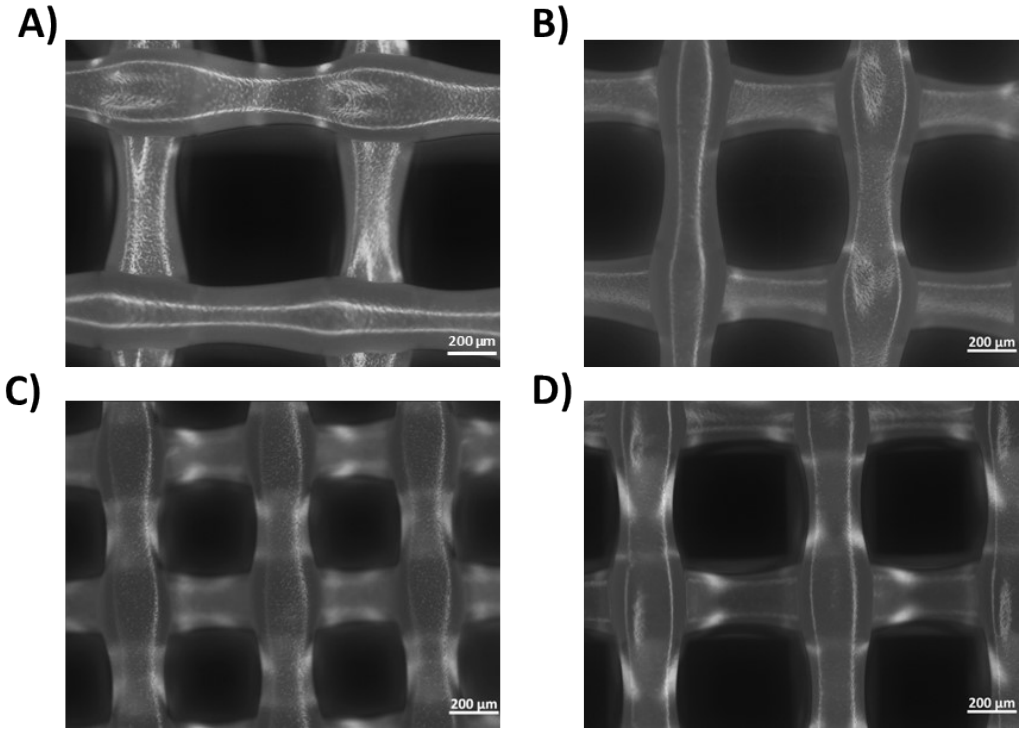

Figure S9. Optical microscopy images of AUPPEG8K scaffolds from the top view. A) Scaffold obtained with printing speed of 250 mm/min and pressure of 3 bar. B) Scaffold obtained with printing speed of 250 mm/min and pressure of 5 bar. C) Scaffold obtained with printing speed of 500 mm/min and pressure of 3 bar. D) Scaffold obtained with printing speed of 500 mm/min and pressure of 5 bar. Scale bar is 200 µm.

Representative images comparing AUPPEG8K scaffolds in the dry and the swollen state are shown in Figure S10.

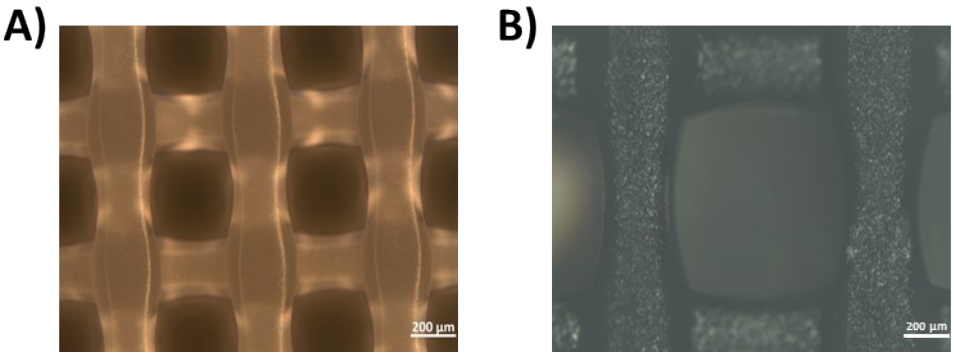

Figure S10. Optical microscopy images of AUPPEG8K scaffolds from the top view. A) AUPPEG8K scaffold with 350 µm PS and 240 µm struts (3D printed with 500 mm/min and 5 bar). B) Swollen state of scaffold depicted in panel A. Scale bar 200 µm.

The comparison between the theoretical and the experimental pore sizes for AUPPEG8K scaffolds is shown in Figure S11A.

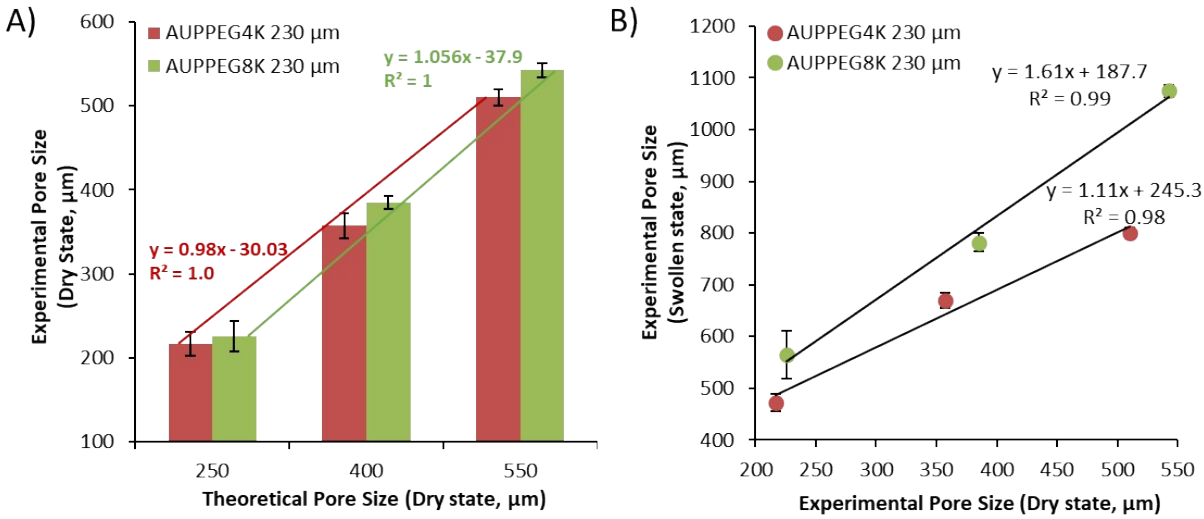

Figure S11. Pore size correlation of AUPPEG8K scaffolds obtained via optical microscopy. A) Theoretical pore size versus experimental pore size for dry scaffolds. B) Experimental pore size of scaffolds in the dry versus hydrated state.

The results reveal that there is a linear correlation between the theoretical and the experimental pore sizes (R^2 = 1.0). The small standard deviations (ranging from 1.6-7.8%) imply that the scaffolds with varying pore sizes can be printed in a reproducible fashion. Furthermore, irrespective of the selected theoretical pore size, a comparison between the experimental and the theoretical (as designed) pore sizes of the AUPPEG8K scaffolds revealed differences ranging from 1.3-9.7%. This can be explained by the ellipsoidal shape of the obtained struts, as schematically illustrated in Figure S12.

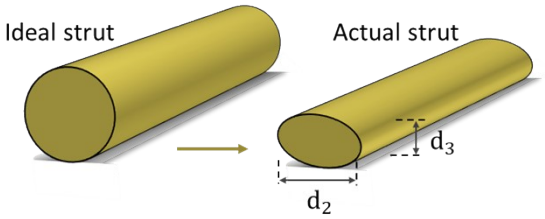

Figure S12. Representative image of ideal and actual AUP struts.

Figure S11B shows the correlation between the pore sizes in the dry and the hydrated state. For the AUPPEG8K scaffolds, there is a linear correlation between pore size in the dry and hydrated state (R^2 of 0.99). Based on these correlations, the experimental pore size of scaffolds in the swollen state can be extrapolated for a specified set of printing parameters. Figures S10 and S11B also show that AUPPEG8K scaffolds swell more compared to AUPPEG4K counterparts, as anticipated. This can be explained by the fact that an increase in the molar mass of the AUP's backbone implies a decrease in the crosslinking density and thus an increase in the distance between crosslinking points, resulting in a higher water uptake capacity for the AUPPEG8K scaffolds.

Finally, we confirmed the interconnectivity of the AUPPEG4K scaffolds by comparing cross-sections at different levels and angles using nano-CT analysis. The data (Figure S13) reveals the scaffolds to be interconnective.

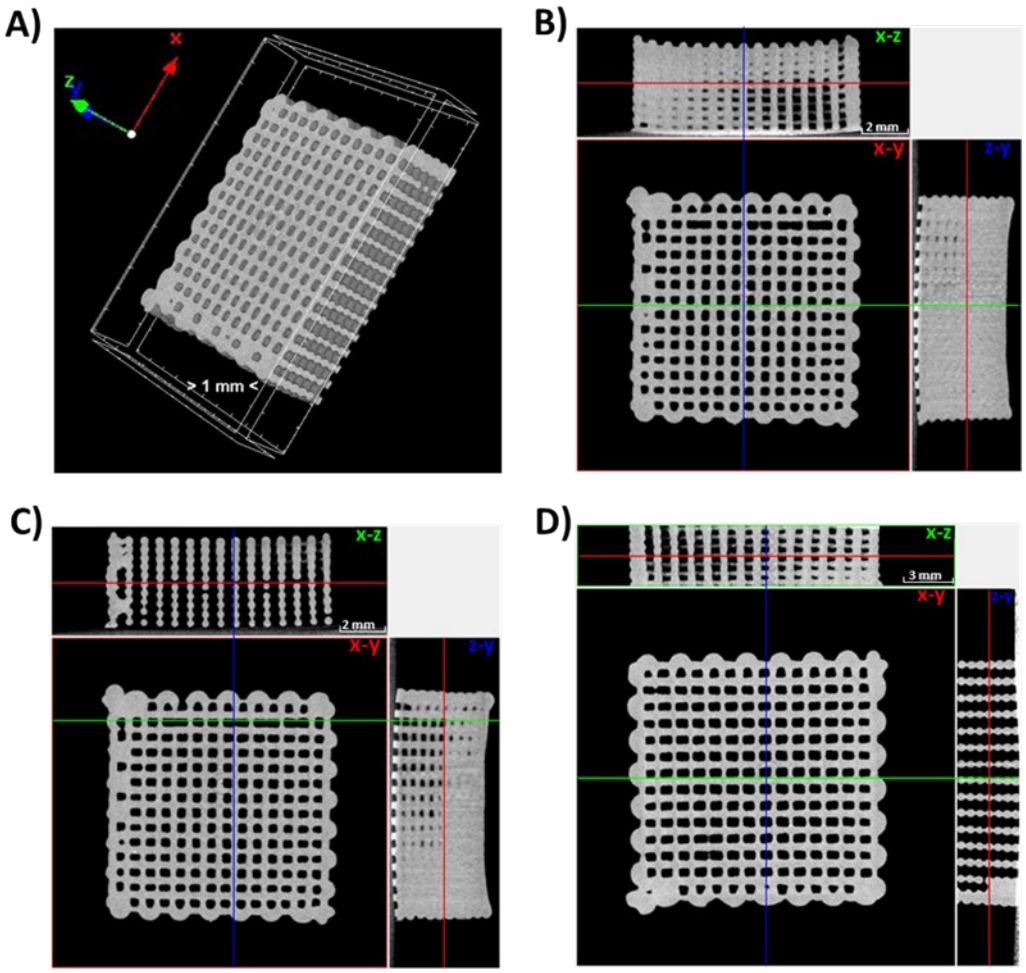

Figure S13. Nano-CT images of AUPPEG4K scaffolds with 350 µm pore size and 370 µm strut diameter. A-D) Cross section of the scaffold in different planes.

8.2 Effect of photo-initiator

First, the effect of the PI concentration (2, 4 and 8 mol % PI with respect to the acrylates present) on the gel fraction and swelling degree of AUPPEG8K scaffolds was investigated. For this, the scaffolds with 510 µm pore size and 230 µm strut diameter were selected (Figure S14A). As expected, the higher PI concentration improved the crosslinking efficiency, resulting in a higher network density, and higher gel fractions. Indeed, values of 70%, 78% and 84% were found in the presence of 2, 4, and 8 mol % PI, respectively. As shown in Figure S14A, the scaffolds reached higher gel fractions (above 75%) in the presence of 4 and 8 mol % PI. Thus, these two PI concentrations were studied further in the selected pore sizes.

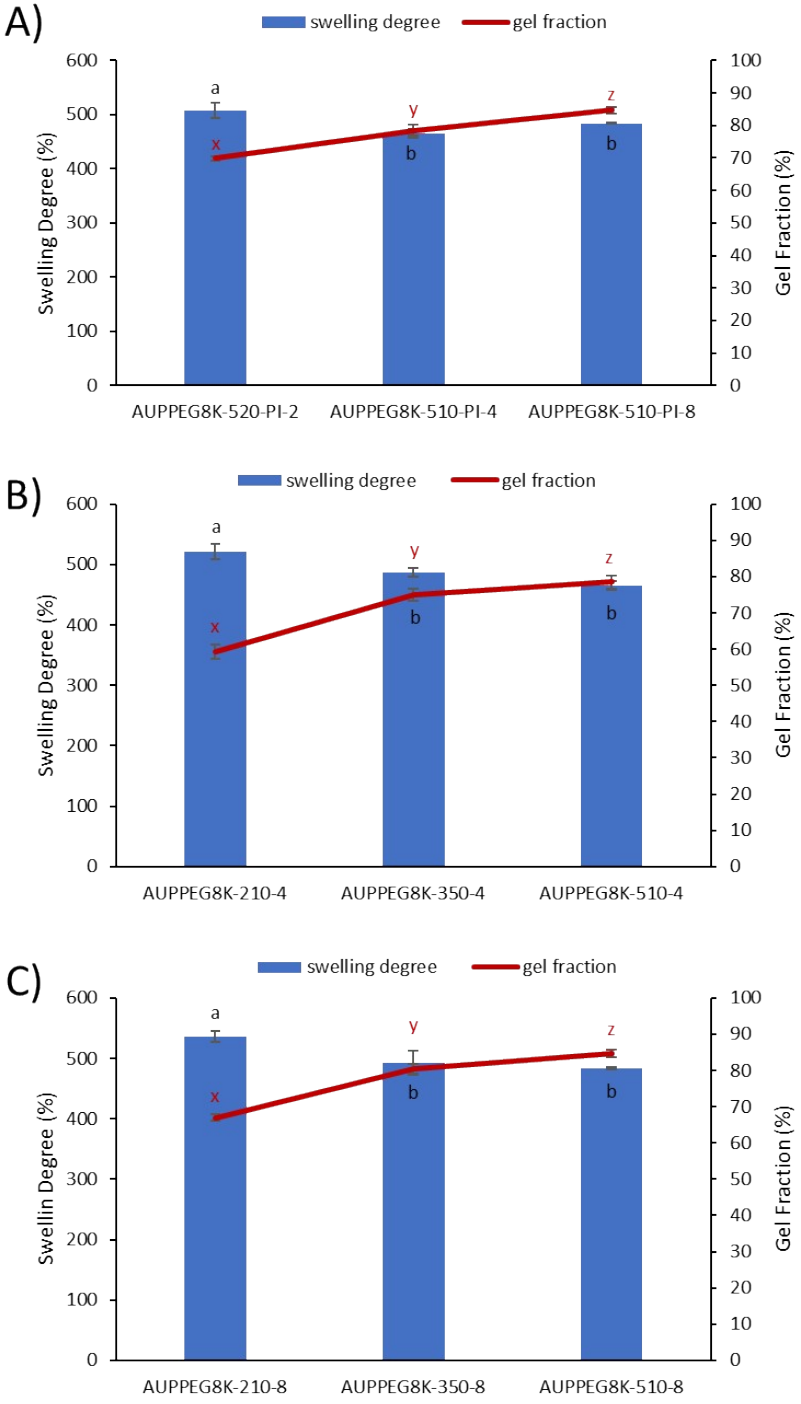

Figure S14. The effect of PI concentration on gel fraction and swelling degree of AUPPEG8K scaffolds with 230 µm strut diameter. A) The effect of PI concentration on scaffolds with 510 µm pore size. B) The effect of pore size on scaffolds in the presence of 4 mol % PI. C) The effect of pore size on scaffolds in the presence of 8 mol % PI. Bars labeled with the same letter (a, b, c) are not significantly different, lines labeled with the same letter (x, y, z) are not significantly different. ($p>0.05$). Statistically significant difference, n=3, $p<0.05$.

In the presence of 4 and 8 mol % PI (Figure S14B and C), the gel fraction increased with increasing pore size. Higher gel fractions indicate higher crosslinked network densities, causing a decrease in water uptake capacity and resulting in lower swelling degrees, as anticipated. The swelling degree ranged between 460 and 530% for AUPPEG8K scaffolds, implying that the scaffolds took up an amount of water

that is 4.6 to 5.3 times their dry weight. From the data, it can also be concluded that the presence of 4 and 8 mol % PI compared to 2 mol % negatively and significantly affects the swelling degree. This finding is linked to the higher crosslinking densities obtained with higher PI concentrations. However, the gel fraction of AUPPEG8K scaffolds with 210 µm pore size was below 70% and it was not significantly affected by a PI concentration increase. This can be attributed to the selected crosslinking method of the scaffolds, in which the applied UV light scattering can decrease the penetration depth and/or the intensity of the UV light, leading to a decrease in the efficiency of the crosslinking reaction. Nevertheless, the gel fractions of AUPPEG8K scaffolds with 350 and 510 µm pore size in the presence of both 4 and 8 mol% PI were above 75%, enabling preservation of their structural integrity. Therefore, the optimal PI concentration of AUPPEG8K scaffolds was selected as 4 mol% for further experiments to prevent any excess use of Irgacure 2959.

Given the lower gel fractions (<70 %) of the AUPPEG8K scaffolds with 210 µm pore size, leading to inadequate structural integrity, these scaffolds were not evaluated for their mechanical properties. The results for the other scaffolds, including their compressive strength, deformation at break and compressive modulus, are shown in Figure S15. The AUPPEG4K counterparts are included to enable comparison. Overall, AUPPEG4K materials are stronger (as reflected by the higher compressive strength and compressive modulus) than their AUPPEG8K counterparts. The latter reveals a larger ductility (as reflected by the higher deformation at break).

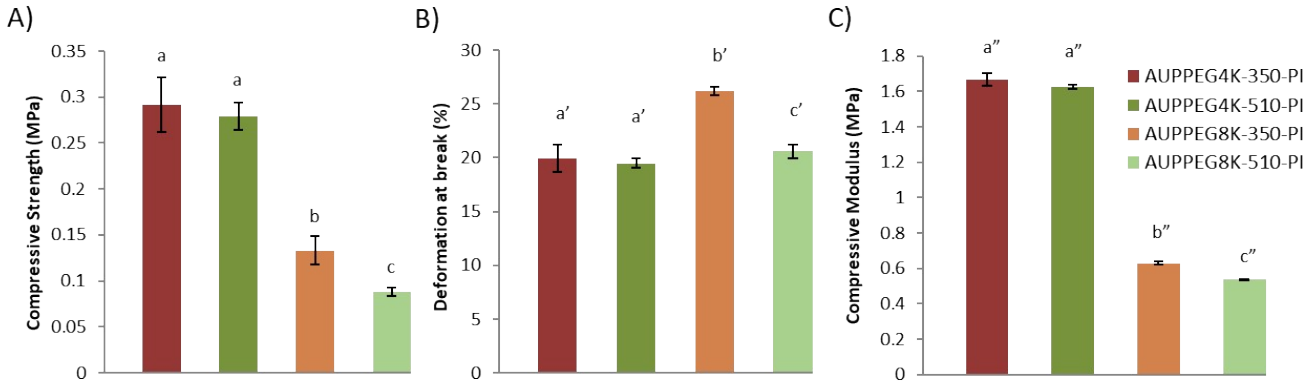

Figure S15. Effect of AUP backbone (PEG) molar mass and pore size on the mechanical properties of AUP scaffolds with 230 µm strut diameter. PI indicates the presence of 2 or 4 mol % Irgacure 2959 relative to the acrylates present in AUPPEG4K and AUPPEG8K scaffolds, respectively. A) Compressive strength. B) Deformation at break. C) Compressive modulus. Bars labeled with the same letter (a, b, c) are not significantly different. Statistically significant difference, n=3, $p<0.05$.

References

1. Yen FS, Lin LL, Hong JL. Hydrogen-bond interactions between urethane−urethane and urethane−ester linkages in a liquid crystalline poly(ester−urethane). Macromolecules. 1999;32(9):3068–79.

2. Goodlett VW. Use of in situ reactions for characterization of alcohols and glycols by nuclear magnetic resonance. Anal Chem. 1965;37(3):431–2.

3. Barbeau Ph, Gerard JF, Magny B, Pascault JP, Vigier G. Morphological analysis of photocured polyurethane acrylate networks. Correlation with viscoelastic properties. J Polym Sci Part B Polym Phys. 1999;37(9):919–37.

4. Kricheldorf HR. Syntheses of biodegradable and biocompatible polymers by means of bismuth catalysts. Chem Rev. 2009;109(11):5579–94.

5. Lomölder R, Plogmann F, Speier P. Selectivity of isophorone diisocyanate in the urethane reaction influence of temperature, catalysis, and reaction partners. J Coat Technol. 1997;69(868):51–7.

6. Sundararajan S, Samui AB, Kulkarni PS. Synthesis and characterization of poly(ethylene glycol) (PEG) based hyperbranched polyurethanes as thermal energy storage materials. Thermochim Acta. 2017;650:114–22.

7. Zhou G, Ma C, Zhang G. Synthesis of polyurethane- g -poly(ethylene glycol) copolymers by macroiniferter and their protein resistance. Polym Chem. 2011;2(6):1409–14.

8. Guo T, Holzberg TR, Lim CG, Gao F, Gargava A, Trachtenberg JE, et al. 3D printing PLGA: a quantitative examination of the effects of polymer composition and printing parameters on print resolution. Biofabrication. 2017;9(2):024101.

9. Aho J, Boetker JP, Baldursdottir S, Rantanen J. Rheology as a tool for evaluation of melt processability of innovative dosage forms. Int J Pharm. 2015;494(2):623–42.

10. Mishra AA, Momin A, Strano M, Rane K. Implementation of viscosity and density models for improved numerical analysis of melt flow dynamics in the nozzle during extrusion-based additive manufacturing. Prog Addit Manuf. 2022;7(1):41–54.